Communication

Gradient Porous Structured MnO₂-Nonwoven Composite: A Binder-Free Polymeric Air Filter for Effective Room-Temperature Formaldehyde Removal

Zijian Dai [1,2]**, Jianyong Yu** [1,2,]*** and Yang Si** [1,2,]***

[1] State Key Laboratory for Modifcation of Chemical Fibers and Polymer Materials, College of Materials Science and Engineering, Donghua University, Shanghai 201620, China; zjdai@dhu.edu.cn

[2] Innovation Center for Textile Science and Technology, Donghua University, Shanghai 200051, China

* Correspondence: yujy@dhu.edu.cn (J.Y.); yangsi@dhu.edu.cn (Y.S.)

Abstract: Recently, MnO₂-coated polymeric filters have shown promising performance in room-temperature formaldehyde abatement. However, a commonly known concern of MnO₂/polymer composites is either MnO₂ crystal encapsulation or weak adhesion. This work reports a low-cost high-throughput and green strategy to produce binder-free MnO₂-nonwoven composite air filters. The production approach is energy saving and environmentally friendly, which combines MnO₂ crystal coating on bicomponent polyolefin spunbond nonwovens and subsequent heat immobilizing of crystals, followed by the removal of weakly bonded MnO₂. The binder-free MnO₂-nonwoven composites show firm catalyst-fiber adhesion, a gradient porous structure, and excellent formaldehyde removal capability (94.5% ± 0.4%) at room temperature, and the reaction rate constant is 0.040 min^{-1}. In contrast to the MnO₂-nonwoven composites containing organic binders, the HCHO removal of binder-free filters increased by over 4%. This study proposes an alternative solution in producing catalyst/fabric composite filters for formaldehyde removal.

Keywords: MnO₂; bicomponent polyolefin nonwovens; polymeric filter; binder-free; HCHO removal

1. Introduction

Formaldehyde (HCHO), one of the major indoor air pollutants, is reported to be continuously emitted from construction and decoration materials [1,2]. In 2004, the International Agency for Research on Cancer (IARC) classified HCHO as carcinogenic to humans (Group 1), as evidence shows that nasopharyngeal cancer and leukemia correlate with exposure to formaldehyde [3,4]. In 2010, the World Health Organization (WHO) set the indoor guideline value for HCHO as 0.1 mg/m^3, which has been adopted by major countries, such as Australia, China, Germany, and Japan [5]. According to a recent study investigating the residential HCHO concentrations in nine provinces in China, almost half (45.7%) of the residences exceeded the WHO limit [6]. Therefore, developing universal room-temperature HCHO treatment approaches is important and welcomed [7–9]. The commonly used catalysts for HCHO abatement include noble metals [10,11], transition metal oxides [12–14], modified carbons [15,16], metal–organic frameworks [17–19], and so on; however, transition metal oxide is the most attractive heterogeneous catalyst in terms of robust performance and low energy consumption.

Among transition metal oxide catalysts, manganese dioxide (MnO₂) is widely used in HCHO heterogeneous catalytic removal as it can readily oxidize HCHO and convert it to H₂O and CO₂ [20–22]. However, MnO₂ crystals are difficult to handle and utilize, not ideal for room-temperature HCHO abatement in practical applications [23]. In this regard, immobilizing MnO₂ on a fibrous substrate is of great interest, because the firm adhesion of MnO₂ on substrates sets a fundamental basis for real applications.

Previous reports on MnO_2-fiber composite filters studied their performance for HCHO removal at room temperature. For example, Wang et al. [24] developed a one-step hydrothermal approach to deposit MnO_2 on polyethylene terephthalate (PET) fibers, allowing over 94% removal efficiency of HCHO (0.6 mg cm^{-3}) at room temperature under a gas hourly space velocity (GHSV) of 90 L g$_{cat}^{-1}$ h^{-1}. Hu et al. [25] produced a MnO_2/polystyrene fibrous structure. Using 5 ppm of HCHO and a GHSV of 60 L g$_{cat}^{-1}$ h^{-1}, the composites enable up to 88.2% HCHO removal efficiency. Additionally, Qu et al. [26] recently reported that utilizing a friction-heating adhesion approach shortened the production time of MnO_2@PET composite. A possible concern with these systems is the low throughput in production, which could add cost to the final product. Organic binders are usually used to bind powderlike catalysts with fibrous substrates at mills. Sekine et al. [27] demonstrated continuous HCHO degradation capability using a fiber cloth filter binding with MnO_2 and activated carbons. However, the catalytic oxidation performance was partially hampered by the organic binders [24]. Besides, binders may also pose a threat to body health in production and utilization [28].

Direct adhesion of MnO_2 on polymeric fabrics remains a challenge for a scalable process. Therefore, it is of great importance to develop a green method that produces catalyst-supported hybrid filters at lower cost and high throughput. Here, we proposed a robust methodology to produce MnO_2-coated fibrous filters by attaching MnO_2 to bicomponent polyolefin (bico-polyolefin) spunbond nonwovens. The bico-polyolefin spunbond nonwovens are made with core component polypropylene (PP) surrounded by sheath component polyethylene (PE). Due to its different melting temperature, a PE sheath will be sufficiently softened and infused to bind MnO_2 crystals at a lower temperature without destroying PP cores; thus, no additional organic binder is required for the system. The binder-free MnO_2-nonwoven composite filters have gradient pore structures and excellent catalytic oxidation ability of HCHO at room temperature.

2. Materials and Methods

2.1. Materials

Potassium permanganate ($\geq$99.5%, $KMnO_4$) was supplied by Shanghai Lingfeng Chemical Reagent Co., Ltd., Shanghai, China. n-Butyl alcohol ($\geq$99.5%, BA) was supplied by Shanghai Titan Scientific Co., Ltd., Shanghai, China. Poly(vinyl alcohol) (PVA) 1788 and HCHO solution ($\geq$36%) were purchased from Shanghai Aladdin Reagent Co., Ltd., Shanghai, China. All reagents were of analytical grade and used without further purification. Hydrophilic bicomponent polyolefin (polyethylene/polypropylene, PE/PP) nonwovens with a basis weight of 110 g m^{-2} were provided by Hangzhou Holyway Co., Ltd., Hangzhou, China. Styrene–acrylic emulsion (SAE, 7199A, solid content, 48.2%) was purchased from Guangzhou Suixin Chemical Co., Ltd., Guangzhou, China.

2.2. Synthesis of MnO_2 Catalysts

MnO_2 crystals were synthesized using reported procedures [29]. Briefly, 37.92 g of $KMnO_4$ was fully dissolved in 600 mL of distilled water under vigorous stirring at room temperature. Then 96 mL of BA was added to the above solution and stirred constantly for 12 h to complete the redox reaction. The synthesized crystals were filtered and washed in deionized water twice, finally dried at 90 °C for 12 h before use.

2.3. Preparation of MnO_2-Nonwoven Composites

To produce binder-free MnO_2-nonwoven composite air filters, a laboratory production line was utilized, as depicted in Figure 1. First, a certain amount of MnO_2 crystals was added to the water tank. After this step, PVA solution was added to the above water tank, which allowed MnO_2 crystals to suspend in solution. The weight percentage of the PVA agent was controlled at 1–3% compared with MnO_2. Then the precursor solution was under vigorous stirring for 10 h to create MnO_2 suspension. After that, one piece of bico-polyolefin nonwoven swatch (11 cm × 12 cm) was soaked into MnO_2 suspension,

and then heated at 135 °C for 3 min after going through the calendering process. When the heating process was completed, the MnO_2-nonwoven composite was washed in a water bath to remove PVA, unbonded MnO_2, and was finally dried at 100 °C (Figure S1). Repeating the above soaking, calendering, heating, and washing steps one more time, the binder-free MnO_2-nonwoven composite was obtained. Using 10%, 15%, and 20% of MnO_2 concentration in solution, the loading amount of MnO_2 in composite air filters ranges from 45 to 66 wt% (Table 1), denoted as 10%MnO_2@Polyolefin, 15%MnO_2@Polyolefin, and 20%MnO_2@Polyolefin, respectively. The uniform dark color of the as-prepared MnO_2-nonwoven composite confirms full coverage of white colored bico-polyolefin spunbond nonwovens (Figure S2).
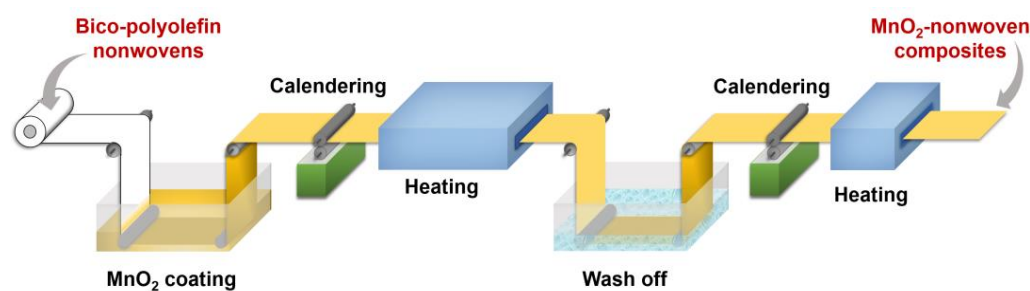
Figure 1. Technological production process of MnO_2-nonwoven composite filters.

Table 1. Preparation details in MnO_2-nonwoven composites.

Sample	Concentration of MnO_2 in Precursor Solution	MnO_2 Content in MnO_2-Nonwoven Composite
10%MnO_2@Polyolefin	10%	45% ± 3%
15%MnO_2@Polyolefin	15%	54% ± 4%
20%MnO_2@Polyolefin	20%	66% ± 4%
MnO_2@binder@Polyolefin	15%	50% ± 3%

As control, another type of MnO_2-nonwoven composite was produced, where MnO_2 was bonded to PE/PP nonwovens with a SAE binder, denoted as MnO_2@binder@Polyolefin. To prepare MnO_2@binder@Polyolefin, 15% of MnO_2 crystals were first added to the water tank and stirred. Then SAE (SAE/MnO_2, 0.4:1, *w/w*) was added under stirring. After that, another PE/PP swatch (11 cm × 12 cm) was soaked into the above solution, calendered, and heated at 90 °C for 5 min.

2.4. Characterization

X-ray diffraction (XRD) pattern was recorded on an XRD tool (D/max-II B, Shimadzu, Kyoto, Japan) to investigate the crystalline structure. Fourier-transform infrared (FTIR) spectroscopy was carried out with a spectrometer (Nicolet iS10, Thermo Fisher, Waltham, MA, USA). The surface morphology of bico-polyolefin spunbond nonwovens and MnO_2-nonwoven composites was investigated using a scanning electron microscope (SEM, SU5000, Hitachi, Tokyo, Japan). The pore size distributions of PE/PP nonwovens and MnO_2-nonwoven composites were evaluated by utilizing a capillary flow porometer (CFP-1100AI, Porous Materials, Inc., Ithaca, NY, USA). The pressure drop of the bico-polyolefin nonwovens and MnO_2-nonwovens composites was measured by employing an automated filter tester (TSI 8130, TSI, Inc., Shoreview, MN, USA).

The formaldehyde (HCHO) removal efficiency of MnO_2-nonwoven composite air filters was measured in the lab-scale setup (Figure S3). The testing samples were placed in a commercial car air purifier (GP5202, Philips, Lumileds (Shanghai) Management Co., Ltd., Shanghai, China), which was then put in an acrylic reactor (0.232 m^3). An amount of 0.7 μL of HCHO solution was injected into the reactor, and then the indoor air was blended by a 5 watt fan, which was fixed on top of the reactor. When the concentration of

HCHO was stabilized to 0.89 ppm, the car air purifier was switched on to start the test. The concentration of HCHO was monitored by a portable gas detector (BSQ-BCH2O, Shanghai Benshan Instrument and Equipment Co., Ltd., Shanghai, China) at 25 °C for 120 min. The HCHO removal performance was evaluated by plotting (C/C_0) versus reaction time, and the reaction rate constant (*k*) was defined as Equation (1):

$$k = \ln\left(\frac{C_0}{C}\right)/t \tag{1}$$

where C_0 (ppm) is the initial concentration of HCHO before the test, and *C* (ppm) is the dynamic concentration of HCHO at different time points.

3. Results and Discussion

3.1. Production and Characterization of MnO$_2$-Nonwoven Composites

The crystallographic structure of MnO$_2$ crystal was identified by using XRD. Figure 2a presents the main diffraction peaks at 12.5°, 25.1°, 36.1°, and 65.4°, which correspond to the characteristic peaks of δ-MnO$_2$ [30].The FTIR spectra show surface features of bico-polyolefin nonwovens and a MnO$_2$@Polyolefin sample. As can be seen from the red spectrum of PE/PP nonwovens in Figure 2b, the peaks at 2914 and 2846 cm^{-1} are assigned to the CH$_2$ asymmetric stretch and CH$_2$ symmetric stretch modes, respectively [31]. Interestingly, the characteristic peaks of low-density polyethylene (LDPE) and high-density polyethylene (HDPE) are all observed on the spectrum of PE/PP nonwovens. The peak located at 1375 cm^{-1} belongs to the CH$_2$ umbrella mode of LDPE, whereas the peaks at 730 and 717 cm^{-1} are split CH$_2$ rocking peaks of HDPE [31,32]. The above results indicate that both of the HDPE and LDPE chips were added to produce a PE sheath component in bico-polyolefin spunbond nonwoven production. It is worth noting that no peak of the PP component is observed in the FTIR spectrum due to the core–sheath feature of bico-polyolefin nonwovens. Compared with the red curve, the MnO$_2$@Polyolefin FTIR spectrum presents additional peaks at 3390, 1637, and 510 cm^{-1}, which are assigned to the stretching vibration of -OH groups, -OH bending mode, and characteristic band of layered manganese oxides, respectively [33].
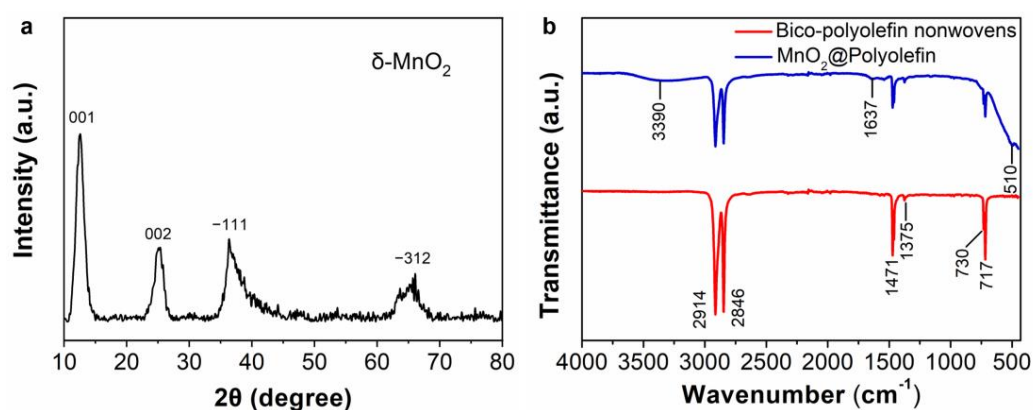

Figure 2. (**a**) XRD pattern of δ-MnO$_2$; (**b**) FTIR spectra of bico-polyolefin spunbond nonwovens and MnO$_2$@Polyolefin filter.

The morphologies of δ-MnO$_2$ crystals, bico-polyolefin nonwovens, and MnO$_2$-nonwoven composites were investigated by SEM. As shown in Figure 3a, δ-MnO$_2$ crystals appear as spherules with an average diameter of 30 nm. The surface of bico-polyolefin nonwovens is relatively smooth compared with the MnO$_2$-nonwovens composites. The bonding points are clearly observed due to the diffusion of the molten PE sheath under appropriate temperature [34]. It can be seen from Figure 3c–e that a MnO$_2$ nanocrystalline is firmly attached to the fiber surface, where the PE component acts as binders and assists in MnO$_2$-fiber adhesion. Notably, when a higher MnO$_2$ concentration is prepared in so-

lution, the coverage areas for bico-polyolefin nonwovens increase significantly. It turns out that 20%MnO$_2$@Polyolefin samples achieved almost full coverage. In contrast, as shown in Figure 3f, when the SAE adhesive was used to bind MnO$_2$, the crystals tended to aggregate on fiber voids. We ascribe the observed particle agglomeration and block to the different surface tension caused by SAE. This is in stark contrast to the binder-free procedure that yields uniform and dense MnO$_2$ coatings on the surface of bico-polyolefin spunbond nonwovens.
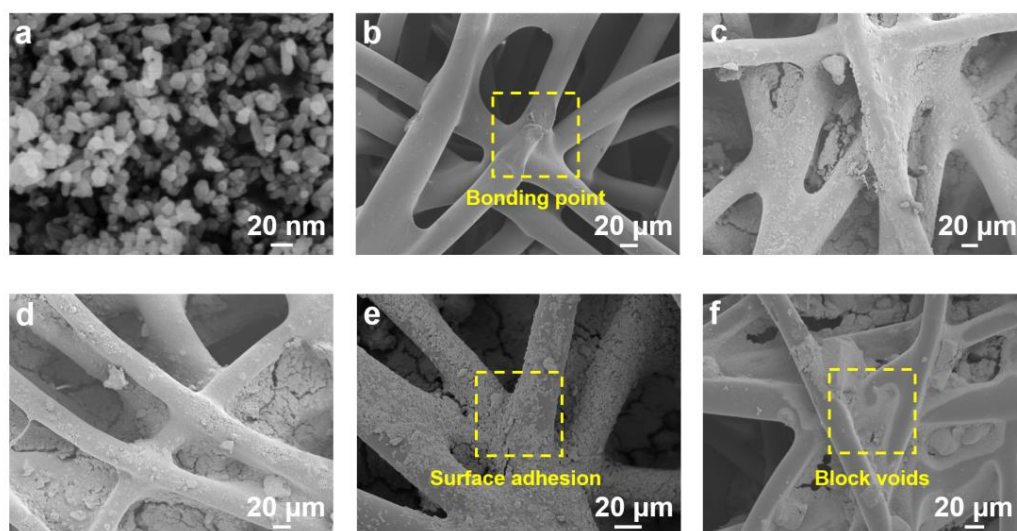
Figure 3. SEM images of (**a**) δ-MnO$_2$, (**b**) bico-polyolefin nonwovens, (**c**) 10%MnO$_2$@Polyolefin, (**d**) 15%MnO$_2$@Polyolefin, (**e**) 20%MnO$_2$@Polyolefin, and (**f**) MnO$_2$@binder@Polyolefin.

3.2. Evaluation of Pore Size Distribution of Bico-Polyolefin Nonwovens and MnO$_2$-Nonwoven Composites

The pore size distribution results for bico-polyolefin nonwovens and MnO$_2$-nonwoven composites are presented in Figure 4a. The bico-polyolefin nonwoven sample shows disordered pore size distribution as several peaks stand out in profile. The addition of MnO$_2$ to the bico-polyolefin nonwovens leads to a narrowed and gradient pore size distribution. Taking 15%MnO$_2$@Polyolefin as an example, it reveals three dominant peaks centered in sequence at around 13, 37, and 63 μm. The mean pore diameter decreases from 67.75 to 52.85 μm compared with the bico-polyolefin nonwovens. We observe that the peak becomes broader and shifts for the MnO$_2$@binder@Polyolefin sample, which gives rise to a further decreased mean pore diameter value, reaching 41.57 μm. However, using SAC adhesive to bind MnO$_2$ did not create a gradient pore distribution for MnO$_2$-nonwoven composites because most of the fiber junctions were blocked, which is consistent with the SEM results in Figure 3f. The results in Figure 4b reflect that the marked increase in pressure drop for MnO$_2$@binder@Polyolefin is also attributed to the blocked pores, and a decreased mean pore diameter correlates with dropped air permeability.

3.3. HCHO Removal Performance of MnO$_2$-Nonwoven Composites

A low concentration HCHO removal performance over MnO$_2$-nonwoven composites was investigated. Figure 5a shows HCHO removal results for 10%MnO$_2$@Polyolefin, 15%MnO$_2$@Polyolefin, and 20%MnO$_2$@Polyolefin. All samples show good HCHO removal efficiency at low concentrations, and 15%MnO$_2$@Polyolefin removed 94.5% ± 0.4% of HCHO within 120 min. Likewise, 10%MnO$_2$@Polyolefin and 20%MnO$_2$@Polyolefin removed 92.5% ± 0.6% and 89.1% ± 0.7%, respectively, in a same time period. The above results indicate that overloading MnO$_2$ crystals on nonwovens hinders the performance of HCHO catalytic removal. As shown in Figure 5b, using binders to produce MnO$_2$-nonwoven composites could not only raise environmental concerns, but also lead to worse

removal performance. The HCHO removal efficiency for the MnO$_2$@binder@Polyolefin sample was reduced by over 4% compared with 15%MnO$_2$@Polyolefin. It is believed that particle agglomeration and encapsulation by an adhesive are the main factors that contribute to worse removal performance. In Figure 5c, we plotted the kinetic curves by measuring ln(C/C_0) versus the reaction time. According to the pseudo-first-order model, the initial rate constants of 10%MnO$_2$@Polyolefin, 15%MnO$_2$@Polyolefin, 20%MnO$_2$@Polyolefin, and MnO$_2$@binder@Polyolefin were 0.030, 0.040, 0.027, and 0.035 min^{-1}, respectively. In addition, 15%MnO$_2$@Polyolefin exhibited impressive reproducibility (Figure 5d) as the HCHO removal performance showed no significant difference after four tests. The HCHO removal performance of selected catalysts is summarized in Table S1, Supporting Information. In comparison with other materials, 15%MnO$_2$@Polyolefin showed acceptable performance in overall HCHO removal.
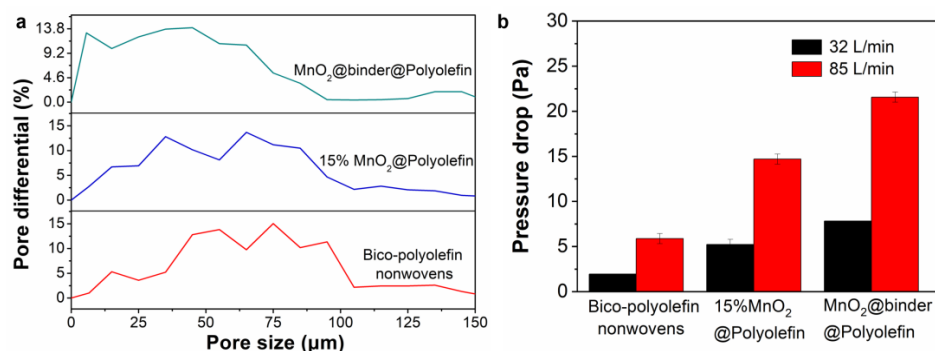
Figure 4. (**a**) Pore size distribution and (**b**) pressure drop of bico-polyolefin nonwovens, 15%MnO$_2$@Polyolefin, and MnO$_2$@binder@Polyolefin.
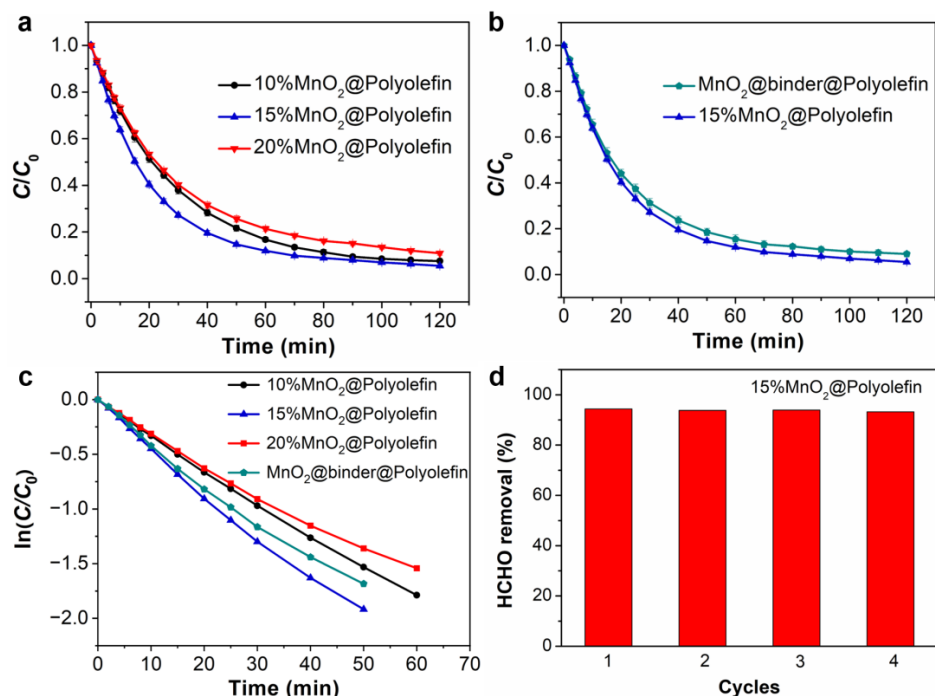
Figure 5. (**a**) HCHO removal test on 10%MnO$_2$@Polyolefin, 15%MnO$_2$@Polyolefin, and 20%MnO$_2$@Polyolefin. (**b**) Comparisons of HCHO removal performance on 15%MnO$_2$@Polyolefin and MnO$_2$@binder@Polyolefin. (**c**) Reaction kinetic curves of 10%MnO$_2$@Polyolefin, 15%MnO$_2$@Polyolefin, 20%MnO$_2$@Polyolefin, and MnO$_2$@binder@Polyolefin for HCHO removal following the pseudo-first-order model. (**d**) Reproducibility tests of HCHO removal performance on 15%MnO$_2$@Polyolefin.

4. Conclusions

In summary, we demonstrated a robust approach to produce binder-free MnO_2-nonwoven composite filters using δ-MnO_2 crystals bonded firmly on the surface of bicomponent PE/PP spunbond nonwovens. The SEM images of MnO_2@Polyolefin samples show that the molten PE component enables MnO_2 to be attached to a fiber surface, whereas nanocrystalline MnO_2 tends to be aggregate at fiber junctions to block inherent pores for MnO_2@binder@Polyolefin. Results of pore size distribution and pressure drop confirm that the gradient porous structures are constructed for MnO_2@Polyolefin filters. Moreover, the HCHO removal test elucidates that binder-free MnO_2@Polyolefin filters show improved HCHO removal performance (94.5% ± 0.4%, $k = 0.040$ min^{-1}) in contrast to MnO_2@binder@Polyolefin filters (90.2% ± 0.9%, $k = 0.035$ min^{-1}). We believe that such a green and environmentally friendly approach will provide an alternative solution in producing catalyst/fabric composite filters.

References

1. Kampa, M.; Castanas, E. Human health effects of air pollution. *Environ. Pollut.* **2008**, *151*, 362–367. [CrossRef] [PubMed]
2. Rong, S.P.; Zhang, P.Y.; Yang, Y.J.; Zhu, L.; Wang, J.L.; Liu, F. MnO_2 Framework for Instantaneous Mineralization of Carcinogenic Airborne Formaldehyde at Room Temperature. *ACS Catal.* **2017**, *7*, 1057–1067. [CrossRef]
3. Nielsen, G.D.; Larsen, S.T.; Wolkoff, P. Re-evaluation of the WHO (2010) formaldehyde indoor air quality guideline for cancer risk assessment. *Arch. Toxicol.* **2017**, *91*, 35–61. [CrossRef] [PubMed]
4. Salthammer, T. Formaldehyde sources, formaldehyde concentrations and air exchange rates in European housings. *Build. Environ.* **2019**, *150*, 219–232. [CrossRef]
5. Salthammer, T.; Mentese, S.; Marutzky, R. Formaldehyde in the Indoor Environment. *Chem. Rev.* **2010**, *110*, 2536–2572. [CrossRef]
6. Huang, S.; Song, S.; Nielsen, C.P.; Zhang, Y.; Xiong, J.; Weschler, L.B.; Xie, S.; Li, J. Residential building materials: An important source of ambient formaldehyde in mainland China. *Environ. Int.* **2022**, *158*, 106909. [CrossRef]
7. Guo, J.; Lin, C.; Jiang, C.; Zhang, P. Review on noble metal-based catalysts for formaldehyde oxidation at room temperature. *Appl. Surf. Sci.* **2019**, *475*, 237–255. [CrossRef]
8. Ye, J.; Yu, Y.; Fan, J.; Cheng, B.; Yu, J.; Ho, W. Room-temperature formaldehyde catalytic decomposition. *Environ. Sci. Nano* **2020**, *7*, 3655–3709. [CrossRef]
9. Na, C.-J.; Yoo, M.-J.; Tsang, D.C.W.; Kim, H.W.; Kim, K.-H. High-performance materials for effective sorptive removal of formaldehyde in air. *J. Hazard. Mater.* **2019**, *366*, 452–465. [CrossRef]
10. Ye, J.; Zhou, M.; Le, Y.; Cheng, B.; Yu, J. Three-dimensional carbon foam supported MnO_2/Pt for rapid capture and catalytic oxidation of formaldehyde at room temperature. *Appl. Catal. B Environ.* **2020**, *267*, 118689. [CrossRef]
11. Nie, L.; Zheng, Y.; Yu, J. Efficient decomposition of formaldehyde at room temperature over Pt/honeycomb ceramics with ultra-low Pt content. *Dalton Trans* **2014**, *43*, 12935–12942. [CrossRef] [PubMed]
12. Wang, J.L.; Li, J.E.; Jiang, C.J.; Zhou, P.; Zhang, P.Y.; Yu, J.G. The effect of manganese vacancy in birnessite-type MnO_2 on room-temperature oxidation of formaldehyde in air. *Appl. Catal. B-Environ.* **2017**, *204*, 147–155. [CrossRef]

13. Liu, F.; Rong, S.P.; Zhang, P.Y.; Gao, L.L. One-step synthesis of nanocarbon-decorated MnO_2 with superior activity for indoor formaldehyde removal at room temperature. *Appl. Catal. B-Environ.* **2018**, *235*, 158–167. [CrossRef]

14. Wang, Z.; Wang, W.Z.; Zhang, L.; Jiang, D. Surface oxygen vacancies on Co_3O_4 mediated catalytic formaldehyde oxidation at room temperature. *Catal. Sci. Technol.* **2016**, *6*, 3845–3853. [CrossRef]

15. Bellat, J.-P.; Bezverkhyy, I.; Weber, G.; Royer, S.; Averlant, R.; Giraudon, J.-M.; Lamonier, J.-F. Capture of formaldehyde by adsorption on nanoporous materials. *J. Hazard. Mater.* **2015**, *300*, 711–717. [CrossRef] [PubMed]

16. Zhu, D.D.; Huang, Y.; Cao, J.J.; Lee, S.C.; Chen, M.J.; Shen, Z.X. Cobalt nanoparticles encapsulated in porous nitrogen-doped carbon: Oxygen activation and efficient catalytic removal of formaldehyde at room temperature. *Appl. Catal. B-Environ.* **2019**, *258*, 117981. [CrossRef]

17. Dai, Z.; Lee, D.T.; Shi, K.; Wang, S.; Barton, H.F.; Zhu, J.; Yan, J.; Ke, Q.; Parsons, G.N. Fabrication of a freestanding metal organic framework predominant hollow fiber mat and its potential applications in gas separation and catalysis. *J. Mater. Chem. A* **2020**, *8*, 3803–3813. [CrossRef]

18. Bian, Y.; Wang, R.T.; Wang, S.J.; Yao, C.Y.; Ren, W.; Chen, C.; Zhang, L. Metal-organic framework-based nanofiber filters for effective indoor air quality control. *J. Mater. Chem. A* **2018**, *6*, 15807–15814. [CrossRef]

19. Dai, Z.; Pradeep, S.; Zhu, J.; Xie, W.; Barton, H.F.; Si, Y.; Ding, B.; Yu, J.; Parsons, G.N. Freestanding Metal Organic Framework-Based Multifunctional Membranes Fabricated via Pseudomorphic Replication toward Liquid- and Gas-Hazards Abatement. *Adv. Mater. Interfaces* **2021**, *8*, 2101178. [CrossRef]

20. Su, J.; Cheng, C.; Guo, Y.; Xu, H.; Ke, Q. OMS-2-based catalysts with controllable hierarchical morphologies for highly efficient catalytic oxidation of formaldehyde. *J. Hazard. Mater.* **2019**, *380*, 120890. [CrossRef]

21. Rong, S.; Zhang, P.; Liu, F.; Yang, Y. Engineering Crystal Facet of α-MnO_2 Nanowire for Highly Efficient Catalytic Oxidation of Carcinogenic Airborne Formaldehyde. *ACS Catal.* **2018**, *8*, 3435–3446. [CrossRef]

22. Yang, R.; Fan, Y.; Ye, R.; Tang, Y.; Cao, X.; Yin, Z.; Zeng, Z. MnO_2-Based Materials for Environmental Applications. *Adv. Mater.* **2021**, *33*, 2004862. [CrossRef] [PubMed]

23. Dai, Z.; Zhu, J.; Yan, J.; Su, J.; Gao, Y.; Zhang, X.; Ke, Q.; Parsons, G.N. An Advanced Dual-Function MnO_2-Fabric Air Filter Combining Catalytic Oxidation of Formaldehyde and High-Efficiency Fine Particulate Matter Removal. *Adv. Funct. Mater.* **2020**, *30*, 2001488. [CrossRef]

24. Wang, J.; Yunus, R.; Li, J.; Li, P.; Zhang, P.; Kim, J. In situ synthesis of manganese oxides on polyester fiber for formaldehyde decomposition at room temperature. *Appl. Surf. Sci.* **2015**, *357*, 787–794. [CrossRef]

25. Hu, M.; Yin, L.; Zhou, H.; Wu, L.; Yuan, K.; Pan, B.; Zhong, Z.; Xing, W. Manganese Dioxide-Filled Hierarchical Porous Nanofiber Membrane for Indoor Air Cleaning at Room Temperature. *J. Membr. Sci.* **2020**, *605*, 118094. [CrossRef]

26. Qu, Y.; Zheng, X.; Ma, K.; He, W.; Wang, S.; Zhang, P. Facile coating of MnO_2 nanoparticles onto polymer fibers via friction-heating adhesion for efficient formaldehyde removal. *Chem. Eng. J.* **2022**, *430*, 132954. [CrossRef]

27. Sekine, Y.; Nishimura, A. Removal of formaldehyde from indoor air by passive type air-cleaning materials. *Atmos. Environ.* **2001**, *35*, 2001–2007. [CrossRef]

28. Kozicki, M.; Guzik, K. Comparison of VOC Emissions Produced by Different Types of Adhesives Based on Test Chambers. *Materials* **2021**, *14*, 1924. [CrossRef]

29. Dai, Z.J.; Su, J.F.; Zhu, X.M.; Xu, K.L.; Zhu, J.; Huang, C.; Ke, Q.F. Multifunctional polyethylene (PE)/polypropylene (PP) bicomponent fiber filter with anchored nanocrystalline MnO_2 for effective air purification. *J. Mater. Chem. A* **2018**, *6*, 14856–14866. [CrossRef]

30. Dai, Z.J.; Yu, X.W.; Huang, C.; Li, M.; Su, J.F.; Guo, Y.P.; Xu, H.; Ke, Q.F. Nanocrystalline MnO_2 on an activated carbon fiber for catalytic formaldehyde removal. *RSC Adv.* **2016**, *6*, 97022–97029. [CrossRef]

31. Smith, B.C. The Infrared Spectra of Polymers II: Polyethylene. *Spectroscopy* **2021**, *36*, 24–29.

32. Krimm, S.; Liang, C.Y.; Sutherland, G.B.B.M. Infrared Spectra of High Polymers. II. Polyethylene. *J. Chem. Phys.* **1956**, *25*, 549–562. [CrossRef]

33. Chen, R.X.; Yu, J.G.; Xiao, W. Hierarchically porous MnO_2 microspheres with enhanced adsorption performance. *J. Mater. Chem. A* **2013**, *1*, 11682–11690. [CrossRef]

34. Liu, J.X.; Zhang, X.; Zhang, H.F.; Zheng, L.; Huang, C.; Wu, H.B.; Wang, R.W.; Jin, X.Y. Low resistance bicomponent spunbond materials for fresh air filtration with ultra-high dust holding capacity. *RSC Adv.* **2017**, *7*, 43879–43887. [CrossRef]